ELSEVIER

Journal of Photochemistry and Photobiology A: Chemistry 148 (2002) 169–176

Journal of Photochemistry and Photobiology A:Chemistry

www.elsevier.com/locate/jphotochem

Photonic efficiency and quantum yield of formaldehyde formation from methanol in the presence of various TiO_2 photocatalysts

Chuan-yi Wang [a,b], Joseph Rabani [c], Detlef W. Bahnemann [a,*], Jürgen K. Dohrmann [b]

[a] *Institut für Solarenergieforschung Hameln/Emmerthal (ISFH), Aussenstelle Hannover, Sokelantstrasse 5, D-30165 Hannover, Germany*
[b] *Institut für Chemie/Physikalische und Theoretische Chemie, Freie Universität Berlin, Takustr. 3, D-14195 Berlin, Germany*
[c] *Department of Physical Chemistry, The Hebrew University of Jerusalem, Jerusalem 91904, Israel*

Received 24 July 2001; received in revised form 12 September 2001; accepted 12 September 2001

Abstract

UV illumination of aqueous TiO_2 suspensions yields hydroxyl radicals which can be trapped by methanol yielding formaldehyde (HCHO). The photonic efficiency of HCHO formation (345 ± 35 nm cw illumination) in aqueous, oxygenated TiO_2 suspensions (2.4 nm diameter TiO_2 particles, Degussa P25 and Sachtleben Hombikat UV 100) containing methanol at pH ca. 1–12 has been determined as well as the respective quantum yield in case of 2.4 nm TiO_2. Differences in the activity of the three photocatalysts have been found and are discussed. The photonic efficiency in the presence of P25 and Hombikat UV 100 depends on the catalyst loading ($g\,l^{-1}$) and the pH. Below $2.5\,g\,l^{-1}$ the photonic efficiency is higher for P25 than for Hombikat UV 100 and vice versa at above $2.5\,g\,l^{-1}$. Optimum pH values for P25 and Hombikat UV 100 resulting in maximum photonic efficiencies (ca. 0.13 for P25 and 0.07 for Hombikat UV 100) are 7.7 and 10.4, respectively. Other than with P25 and Hombikat UV 100, which scatter light strongly, the quantum yield of HCHO formation in the colloidal 2.4 nm TiO_2 suspension varies but little with the pH and virtually does not change with the photocatalyst loading (0.1–1.0 g/l). Employing these colloidal particles as photocatalysts the quantum yield varies as the inverse square root of light intensity. It increases from 0.02 to 0.08 when the absorbed photon flux decreases from 8.1×10^{-7} to 4.9×10^{-8} Einstein $l^{-1}\,s^{-1}$. A simple model is presented to explain this observation.

Keywords: TiO_2 photocatalysis; Methanol; Formaldehyde; OH radical; Photonic efficiency; Quantum yield

1. Introduction

Photocatalytic detoxification reactions employing light-absorbing semiconductors have attracted considerable attention in the last 20 years as a potential solution to global environmental problems [1–12]. Several oxide and sulfide semiconductors (e.g., TiO_2, Fe_2O_3, ZnO and CdS) have been used as photocatalysts. TiO_2, however, has proven most suitable for environmental applications because it is highly photoactive, cheap, non-toxic, chemically and biologically inert and photostable [3,4].

The mechanism of TiO_2 photocatalysis has been an objective of extensive research [1–13]. The details of the mechanism vary according to the substrate to be photo-oxidized. Hence, the nature of the leading oxidizing species (surface-bound or quasi-free hydroxyl radicals from the reaction of photogenerated holes with adsorbed hydroxide ions or water molecules, deeply trapped holes, photo-holes in the valence band) active in interfacial charge transfer to the adsorbed substrate molecule or ion must also depend on the properties of the latter since all the oxidizing species originate from photogenerated valence band holes in a competitive manner [14]. Nevertheless, this key feature of TiO_2 photocatalysis has been discussed controversially [13–16]. It is therefore advisable to study the quantum yield or the photonic efficiency for the photocatalytic oxidation of small, weakly adsorbed molecules (e.g., aliphatic alcohols [17]) to obtain a measure for the photogeneration rate of the leading oxidizing species interacting with such a substrate on various TiO_2 catalysts. This is the approach of the present work where methanol has been chosen as a model compound thought to be oxidized by hydroxyl radicals [18].

Recently, Sun and Bolton [18] determined the quantum yield of photochemical hydroxyl radical generation in systems containing powdered TiO_2 (anatase, 100–210 nm in diameter) by employing methanol as an $OH^\bullet$ trap. Methanol is converted to formaldehyde by $OH^\bullet$ attack and further

* Corresponding author. Present address: Institut fuer Technische Chemie, Universitaet Hannover, Callinstrasse 3, D-30167 Hannover, Germany, Tel.: +49-511-7625560; fax: +49-511-7623004.
E-mail addresses: rabani@vms.huji.ac.il (J. Rabani), bahnemann@iftc.uni-hannover.de (D.W. Bahnemann), dohrmann@chemie.fu-berlin.de (J.K. Dohrmann).

1010-6030/02/$ – see front matter
PII: S1010-6030(02)00087-4

oxidation, by O_2 or charge-injection to the CB of TiO_2, of the first-formed $^{\bullet}CH_2OH$. Formaldehyde was assayed by HPLC, and the absorbed photon flux in the light-scattering TiO_2 particulate suspension was obtained by use of an integrating sphere [18]. In the present work we compare the photocatalytic activity of colloidal TiO_2 particles (2.4 nm in diameter) with that of two commercially available photocatalysts, namely Degussa P25 and Sachtleben Hombikat UV 100, by determination of the photonic efficiency[1] and the quantum yield (2.4 nm TiO_2), respectively, of formaldehyde generated by photocatalytic oxidation of methanol in aqueous suspension. Since these quantities reflect the production rate of hydroxyl radicals in the reaction system [18], more insight is gained into the environmental implications and applications of these TiO_2 photocatalysts. The effect of several other important factors such as catalyst loading, pH and photon flux on the photocatalytic activity is also reported.

2. Experimental

Chemicals including $TiCl_4$ (Merck-Schuchardt), CH_3OH, $HClO_4$ and NaOH from Merck (analytical grade reagents), 2,4-dinitrophenylhydrazine (DNPH, Aldrich), TiO_2 P25 (Degussa) and TiO_2 Hombikat UV 100 (Sachtleben Chemie) were used as supplied. Water was purified by a Milli-Q/RO system (Millipore) and had a resistivity of larger than 18 MΩ cm.

Colloidal TiO_2 was prepared by controlled hydrolysis of $TiCl_4$ as reported by Kormann et al. [19]. As-prepared colloidal TiO_2 comes as a white or slightly yellowish crystal-like powder which can be resuspended in water, methanol or in a mixture of both solvents. The colloidal suspension is optically transparent in the visible and does not scatter the incident light noticeably [15,19]. The particle diameter is ca. 2.4 nm as deduced from transmission electron micrographs.

The commercial photocatalysts, P25 (Degussa) and Hombikat UV 100 (Sachtleben Chemie), were used without further pretreatment. The catalysts were suspended in ultrapure water (resistivity > 18 MΩ cm). Prior to measurements the suspensions were sonicated for 30 min. Extinctance spectra of the suspensions, in a 1 mm cuvette, were taken on a Perkin Elmer Lambda-9 spectrophotometer equipped with an integrating sphere.

The photolyzing light was provided by a Xe-lamp (Osram XBO 450). The wavelength range 310–390 nm (maximal intensity at ca. 345 nm) was selected by band pass filters (black + WG 320). The light intensity was adjusted by neutral density filters. Photolyses were carried out in 50 ml spherical or 30 ml cylindrical cells equipped with flat optical-grade quartz windows. Results were invariant with respect to the reactor geometry. The determination of the incident photon flux by chemical actinometry (Aberchrome 540 [20]) was performed in the same cells, thus avoiding the necessity of corrections for any influence of light reflection, beam position and reactor geometry. The pH values of the suspensions to be photolyzed were adjusted by $HClO_4$ or NaOH. All the suspensions were saturated with oxygen and were studied at room temperature. The suspensions were prephotolyzed for 15 min before the addition of methanol.

The amount of HCHO formed by photocatalytic oxidation of methanol was determined by HPLC after reacting HCHO with 2,4-dinitrophenylhydrazine to give the corresponding hydrazone which absorbs at 360 nm [18,21]. HPLC employed a Dionex 4500i chromatograph equipped with a 250 mm reverse-phase column (Nucleosil-100-10C18, 4 mm ID, Macherei & Nagel, Germany). The eluent consisted of CH_3OH, H_2O and CH_3COOH (100:100:1, v/v). The detector was set at 360 nm.

The optical absorbance of the colloidal TiO_2 suspension and of the band pass filters was measured with an Omega spectrophotometer (Bruins Instruments). The relative error of the measured concentration of HCHO was $\leq \pm 8\%$ as judged from repeated runs under identical conditions of photolysis.

3. Results

Illumination of the aqueous TiO_2 suspensions containing methanol and oxygen leads to the formation of formaldehyde (HCHO), the concentration of which increases virtually linearly with illumination time (Fig. 1) when prephotolysis (ca. 15 min) was applied before the addition of methanol. The photolyses were carried out in a 50 ml spherical cell (50 mm diameter) equipped with a flat quartz window (35 mm diameter). The optical path length was between 42 and 50 mm resulting in a maximal absorbance of 0.25 for colloidal TiO_2 (0.1 g l^{-1}) at 345 nm. No formaldehyde was

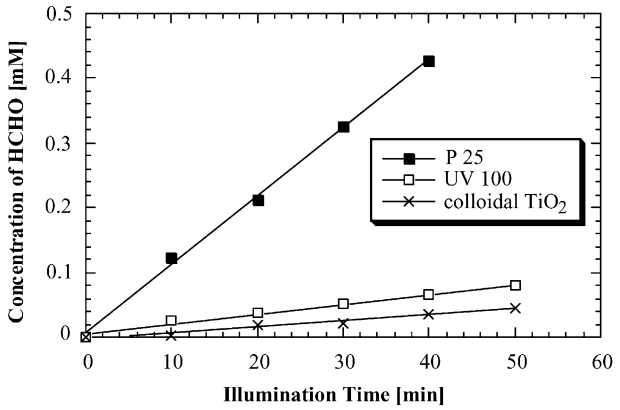

Fig. 1. Effect of illumination time on the concentration of HCHO formed by photocatalytic oxidation of CH_3OH (30 mM) in O_2-saturated aqueous suspension of 2.4 nm TiO_2 particles, Degussa P25 and Hombikat UV 100. λ = 310–390 nm, $I_0 = 3.37 \times 10^{-6}$ Einstein l^{-1} s^{-1}, 0.1 g l^{-1} catalyst loading, pH = 3.5 (see text for analytical method).

[1] The photonic efficiency refers to the incident photon flux, while the quantum yield refers to the flux of photons absorbed by the catalyst.

Table 1
Rate (r) and photonic efficiency (η) of HCHO formation in the systems containing colloidal TiO_2, P25 and Hombikat UV 100 (for conditions, see Fig. 1)

System	r^a ($\times 10^8$ mol l^{-1} s^{-1})	η^b ($\times 10^2$)	η (relative to colloidal TiO_2)
P25/CH_3OH	19.10	5.70	11.8
UV 100/CH_3OH	2.83	0.84	1.8
Colloidal TiO_2/CH_3OH	1.62	0.48[c]	1.0

[a] ±10%.
[b] $\eta = r/I_0$, where I_0 is the incident photon flux in units of Einstein l^{-1} s^{-1}.
[c] From the fraction of light observed by 0.1 g l^{-1} colloidal TiO_2 the quantum yield is $\Phi = 0.02$ as calculated by $\Phi = h/F_s$, where $F_s = 0.238$.

detected after keeping the system in the dark. HPLC did not disclose photolysis products other than formaldehyde.

From Fig. 1 the production rate (r) of HCHO and the photonic efficiency (η) were derived as listed in Table 1. The photonic efficiency obtained for P25 is much higher than for UV 100 and colloidal TiO_2. Since light-scattering is negligible in the latter system [15,19], the quantum yield of HCHO formation could be determined as $\Phi = 0.02$ for $I_0 = 3.37 \times 10^{-6}$ Einstein l^{-1} s^{-1} by making use of the following relation:

$$\Phi = \frac{\eta}{F_s} \quad (1)$$

where $\eta = r/I_0$ is the photonic efficiency and F_s is given by [18]

$$F_s = \frac{\int_{\lambda_1}^{\lambda_2} I_\lambda T_\lambda^f f_\lambda^s \, d\lambda}{\int_{\lambda_1}^{\lambda_2} I_\lambda T_\lambda^f \, d\lambda} \quad (2)$$

where I_λ is the relative incident photon flux in the wavelength band dλ, T_λ^f the transmittance of the filter set at wavelength λ and

$$f_\lambda^s = 1 \pm 10^{\pm A_\lambda^s} \quad (3)$$

is the fraction of light absorbed, where A_λ^s is the measured absorbance of the colloidal TiO_2 sample at wavelength λ.

For the light-scattering suspensions (P25 and Hombikat UV 100) only the photonic efficiency is given in Table 1. Fig. 2 shows the extinction as a function of wavelength

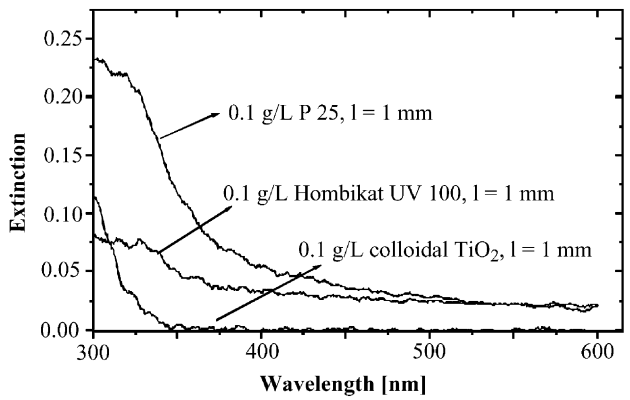

Fig. 2. Extinction spectra of aqueous suspensions (0.1 g l^{-1}) of 2.4 nm colloidal TiO_2, Degussa P25 and Hombikat UV 100 taken by use of an integrating sphere (0.1 cm cuvette, room temperature).

measured for the three photocatalysts (loading 0.1 g l^{-1} in aqueous suspension) by use of an integrating sphere and a 1 mm cuvette (Perkin Elmer Lambda-9). The spectra demonstrate vast differences in the optical properties. While the colloidal TiO_2 particles form a suspension transparent at $\lambda > 400$ nm, there is residual extinction at $\lambda > 450$ nm for P25 and Hombikat UV 100. Due to the anatase modification of these photocatalysts ($\lambda_g = 384$ nm for bulk anatase, $E_g = 3.23$ eV [22]) the residual extinction (ca. 0.025) cannot be attributed to absorption of light. It rather indicates some back-scattering of light from the 1 mm path length suspension not seen (and not compensated for) by the detector placed at the exit slit of the integrating sphere. Hence a rough estimate of the absorbance spectra of the suspensions of P25 and Hombikat UV 100 can be made by considering the residual extinction (0.025) at $\lambda > 500$ nm as the proper zero-line for light absorption [15]. In this manner and by use of Eqs. (2) and (3) the factor F_s was estimated as ca. 0.99 for P25 and 0.87 for Hombikat UV 100 at a loading of 0.1 g l^{-1} and for the average optical path (4.5 cm) of the spherical reactor used here for the photolyses. From Eq. (1) and the values of η (Table 1) the following estimate is obtained for the quantum yield of HCHO formation: $\Phi \approx 0.06$ for P25 and $\Phi \approx 0.01$ for Hombikat UV 100 at a loading of 0.1 g l^{-1} and $I_0 = 3.37 \times 10^{-6}$ Einstein l^{-1} s^{-1}. Hence, P25 is clearly the most active photocatalyst for HCHO formation from CH_3OH under these conditions. It should be noted, however, that a precise determination of the quantum yield in the presence of P25 and Hombikat UV 100 would require application of the more elaborate technique for elimination of light-scattering developed by Sun and Bolton [18] as well as consideration of the, supposedly small, influence of a non-uniform light intensity distribution in slurry photocatalytic reactors [23,24]. This, however, was beyond the scope of the present work.

Cabrera et al. [25] reported specific absorption coefficients, κ^*, for aqueous suspensions of P25 and Hombikat UV 100 which exhibit a spectral dependence similar to the absorbance deduced from Fig. 2. However, κ^* from Ref. [25] is smaller by factors of ca. 0.15 and 0.25 for P25 and Hombikat UV 100 at $\lambda = 350$ nm, respectively, than calculated from our spectra. (From Fig. 2 at 350 nm, κ^* (cm^2 g^{-1}) is ca. 2.2×10^4 for P25 and 0.57×10^4 for Hombikat UV 100 as compared with 0.34×10^4 and 0.14×10^4, respectively, from Fig. 5 of Ref. [25].) This may point to incomplete elimination of light-scattering by our procedure and/or different

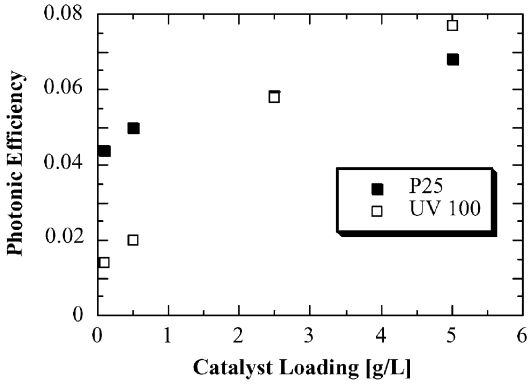

Fig. 3. Effect of loading on the photonic efficiency of the photocatalytic HCHO formation in the presence of P25 and Hombikat UV 100 (30 mM CH_3OH, 10 mM KNO_3, O_2-saturated suspension, pH 3.6, $I_0 = 3.37 \times 10^{-6}$ Einstein l^{-1} s^{-1}, $\lambda = 310$–390 nm).

sample properties (e.g., presence of impurities, differences in particle size and preparation of the suspensions). It should be noted that use of smaller values of κ^* would result in values of Φ_{HCHO} larger than given in the previous paragraph. The conclusions as to the different photocatalytic efficiency of P25 and Hombikat UV 100 would remain the same.

Both P25 and Hombikat UV 100 have been widely used as photocatalysts with respective preference in different cases [26,27]. Fig. 1, Table 1 and the above estimate of the quantum yields show that at low loading (0.1 g l^{-1}) P25 is more efficient than Hombikat UV 100 and colloidal TiO_2 for the photocatalytic oxidation of methanol. However, the situation changes with higher loading. As shown in Fig. 3 the photonic efficiency of Hombikat UV 100 drastically increases with increasing loading and becomes even larger than that for P25 at a loading higher than 2.5 g l^{-1}. A similar phenomenon has been observed in this laboratory for the photodegradation of dichloroacetic acid [26]. Other than with P25 and Hombikat UV 100 the loading of colloidal TiO_2 does not influence the quantum yield of formaldehyde formation (Table 2). This is similar to the finding reported by Sun and Bolton [18] who used TiO_2 particulates (anatase) as a photocatalyst at low light intensity.

Table 2
Effect of pH and catalyst loading on the quantum yield of HCHO formation in the presence of 2.4 nm colloidal TiO_2 (0.1 M CH_3OH in O_2-saturated suspension, cylindrical reactor (l = 3 cm), $I_0 = 1.43 \times 10^{-6}$ Einstein l^{-1} s^{-1}, $\lambda = 310$–390 nm)

pH	0.1 g l^{-1} TiO_2		1.0 g l^{-1} TiO_2	
	F_s (Eq. (2))	Φ_{HCHO} (Eqs. (1) and (2))	F_s (Eq. (2))	Φ_{HCHO} (Eqs. (1) and (2))
1	0.370	0.017	0.830	0.016
2	0.523	0.020	0.843	0.019
10	0.474	0.024	0.843	0.024

The quantum yield and the photonic efficiency of HCHO formation in the presence of colloidal TiO_2 (Table 2) and P25/Hombikat UV 100 (Fig. 4), respectively, depend on the pH of the suspension. The effect is more pronounced in the case of P25 and Hombikat UV 100 where the photonic efficiency has maximal values at pH ca. 7.7 and 10.4, respectively (Fig. 4). This may reflect different acid–base properties of the photocatalysts. As discussed above, the photonic efficiency given in Fig. 4 should not be much different from the quantum yield of HCHO formation. It can therefore be concluded that, at a loading of 0.1 g l^{-1}, P25 is the most active photocatalyst in the pH range 3.5–11.5 among the materials studied here.

The quantum yield of HCHO formation in the presence of colloidal TiO_2 was found to be inversely proportional to the square root of the absorbed photon flux, I_a, in the range of ca. 0.36×10^{-7} to 8.3×10^{-7} Einstein l^{-1} s^{-1} studied (Fig. 5). I_a was adjusted by use of neutral density filters. The straight-line fit in Fig. 5 has a correlation coefficient of 0.97. At the lowest photon flux applied (ca. 4×10^{-8} Einstein l^{-1} s^{-1}) a quantum yield of 0.07 ± 0.006

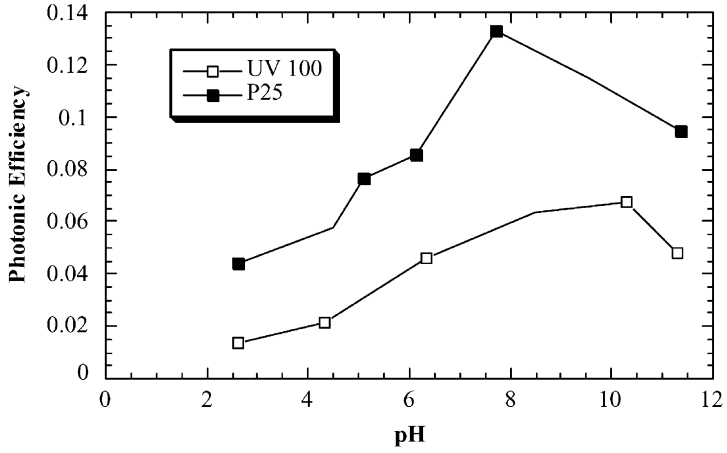

Fig. 4. Influence of pH on the photonic efficiency of HCHO formation in P25 and Hombikat UV 100 suspensions at 0.1 g l^{-1} loading (30 mM CH_3OH, 10 mM KNO_3, O_2-saturated suspension, $I_0 = 3.37 \times 10^{-6}$ Einstein l^{-1} s^{-1}, $\lambda = 310$–390 nm).

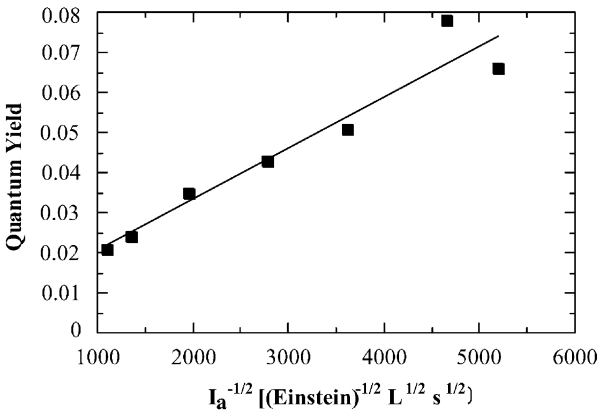

Fig. 5. Dependence of the quantum yield of HCHO formation on the absorbed photon flux in the presence of 2.4 nm colloidal TiO_2 (0.1 M CH_3OH, 0.11 g l^{-1} TiO_2 in O_2-saturated aqueous suspension, pH 3.5, l = 310–390 nm).

was obtained. The inverse square root dependence (Fig. 5) parallels the finding by Sun and Bolton [18] who reported $\Phi_{HCHO} \approx \Phi_{OH^\bullet} \approx 0.04$ for the photocatalytic oxidation of CH_3OH in an aqueous suspension of powdered anatase under comparable conditions. A linear Φ vs. $I_a^{-1/2}$ dependence has also been found by Kormann et al. [28] for the photocatalytic degradation of chloroform in aqueous suspensions of TiO_2.

4. Discussion

4.1. Primary photocatalytic processes and kinetic analysis

The following processes in the TiO_2-photocatalyzed oxidation of aqueous methanol and some simple kinetic considerations can explain the inverse square root dependence of the quantum yield of HCHO formation, Φ_{HCHO}, on the absorbed photon flux, I_a, shown in Fig. 5 for 2.4 nm TiO_2 particles in the presence of oxygen [4,18,29]:

$$TiO_2 + h\nu(\geq E_g) \overset{\text{(fs)[4]},I_a}{\rightarrow} h_{VB}^{+} + e_{CB}^{-} \quad (4)$$

$$h_{VB}^{+} + e_{CB}^{-} \overset{k_2\text{(fast)[4]}}{\rightarrow} TiO_2 + \text{heat} \quad (5)$$

$$h_{VB}^{+} + \equiv Ti^{IV}OH/H_2O \overset{k_3\text{(fast)[4]}}{\rightarrow} \equiv Ti^{IV}OH^{\bullet+}/(OH^\bullet + H^+) \quad (6)$$

$$e_{CB}^{-} + \equiv Ti^{IV}OH \overset{(<0.1\,\text{ns})[4]}{\rightarrow} \equiv Ti^{III}OH/e_{tr}^{-} \quad (7)$$

$$e_{tr}^{-} + O_2 \overset{k_5}{\rightarrow} O_2^{\bullet-} \quad (8)$$

$$OH^\bullet + CH_3OH \overset{k_6}{\rightarrow} {}^\bullet CH_2OH + H_2O \quad (9)$$

$${}^\bullet CH_2OH + O_2 \overset{k_7}{\rightarrow} HCHO + HO_2^\bullet \quad (10)$$

$${}^\bullet CH_2OH + \equiv Ti^{IV}OH \overset{\text{(fast)[29]}}{\rightarrow} HCHO + \equiv Ti^{III}OH/e_{tr}^{-} + H^+ \quad (11)$$

Absorption by TiO_2 particles of UV photons ($h\nu \geq$ bandgap energy) at a rate proportional to the absorbed photon flux, I_a, produces photo-holes, h_{VB}^{+}, and electrons, e_{CB}^{-}, see reaction (4). These charge carriers may either undergo undesired recombination, reaction (5), or they may migrate to the particle surface where they are trapped, see reactions (6) and (7). To simplify the following kinetic analysis, any subsequent reactions of the superoxide radical formed via reaction (8) have been ignored which is justified since both, the superoxide radical as well as its protonated form, are known to be very weak oxidents in aqueous systems [4]. For the present analysis trapping of h_{VB}^{+} is taken to give mobile $OH^\bullet$ as the leading oxidizing species [15,30] which react with CH_3OH by H-atom abstraction, reaction (9) [18]. This process is fast in homogeneous aqueous solution, $k_6 = 5 \times 10^8$ M^{-1} s^{-1} [31]. The resulting ${}^\bullet CH_2OH$ is known either to be further oxidized by O_2 ($k_7 \approx 5 \times 10^9$ M^{-1} s^{-1} [32]) or to inject the unpaired electron into the TiO_2 conduction band, reaction (11) [29]. Both the reactions (10) and (11) form HCHO which is the only product detected under the conditions of the present study.

In the following simplistic analysis it is assumed that the overall production rate of HCHO is controlled by the slow rate of reduction of O_2 by trapped electrons [18,33–35], reaction (8), for which k_5 has been determined as 7.6×10^7 M^{-1} s^{-1} for the colloidal TiO_2 particles used here [14]:

$$\frac{d[O_2^{\bullet-}]}{dt} = k_5[e_{tr}^{-}][O_2] \quad (12)$$

$[e_{tr}^{-}]$ in Eq. (12) can be approximated by the total steady-state concentration of photogenerated electrons, $[e^-]$, since reaction (7) is fast while reaction (8) is slow, i.e. rate-controlling. Similarly, due to the small quantum yield of $OH^\bullet$ in reaction (6) which, according to Sun and Bolton [18], is proportional to the steady-state quantum yield of HCHO, the rate of e^-/h^+-recombination, $k_2[e^-][h^+]$, can be approximated by considering $[h^+]$ as being close to the total steady-state concentration of photogenerated holes. Hence, $[e^-]$ can be obtained from the following steady-state relation:

$$I_a - k_5[e^-][O_2] - k_2[e^-][h^+] \approx 0 \quad (13)$$

The small quantum yield of HCHO measured in the present case (Fig. 5) further implies that most of the photogenerated charge carriers are consumed by recombination. Hence, the second term in Eq. (13), which represents the rate-controlling reduction of O_2, can be neglected. For $[e^-] \approx [h^+]$ in the photostationary state, Eq. (13) reduces to

$$[e^-] \approx \left(\frac{I_a}{k_2}\right)^{1/2} \quad (14)$$

Use of Eq. (14) in Eq. (12) and of the above relation $[e_{tr}^{-}] \approx [e^-]$ yields

$$\frac{d[O_2^{\bullet -}]/dt}{I_a} \approx k_5 k_2^{-1/2}[O_2] I_a^{-1/2} \quad (15)$$

where $(d[O_2^{\bullet -}]/dt)/I_a$ is the quantum yield of the formation of $O_2^{\bullet -}$. In the photostationary state the rates of O_2 reduction and of the oxidation of CH_3OH to $^{\bullet}CH_2OH$, reactions (8) and (9), respectively, must be equal for keeping the electrical potential of the illuminated TiO_2 particles constant by balancing the cathodic and anodic one-electron partial currents flowing through the particle–solution interface [29]. This implies that $\Phi_{O_2^{\bullet -}} = \Phi_{OH^{\bullet}}$. Since $\Phi_{HCHO} = a\Phi_{OH^{\bullet}}$ (with $a \approx 0.93$ [18]) one obtains from Eq. (15)

$$\Phi_{HCHO} \approx a k_2^{-1/2} k_5 [O_2] I_a^{-1/2} \quad (16)$$

Eq. (16) is in agreement with observation as shown in Fig. 5. From the slope of the straight line, $k_{obs} = a k_2^{-1/2} k_5 [O_2]$ is obtained as 1.4×10^{-5} Einstein$^{1/2}$ l$^{-1/2}$ s$^{-1/2}$ for O_2-saturated solution. Note that in the above analysis the reasonable assumption has been made that the sequential reactions (9)–(11) are fast as compared with the rate of formation of mobile $OH^{\bullet}$ by reaction (6).

The quantum yield of HCHO formation determined in the present study is comparable to that of hydroxyl radical and HCHO formation reported for similar conditions by Sun and Bolton [18]. They used powdered anatase as a photocatalyst and also found that the quantum yield was proportional to $I_a^{-1/2}$. However, there are some features in the above analysis which need further consideration. From k_{obs} given above the rate coefficient for e^-/h^+-recombination is estimated as $k_2 = 4 \times 10^{19}$ l mol^{-1} s^{-1}. This value refers to the mole number of photoelectrons present, in the steady state, in 1 l of the photolyzed solution. Conversion to the average concentration of photoelectrons stored in the TiO_2 particles (the loading of 0.1 g l^{-1} corresponds to a particle concentration of 4.7 μmol l^{-1}) gives a rate coefficient of 8×10^{14} l mol^{-1} s^{-1}. This value is more than three orders of magnitude larger than that reported for e^-/h^+-recombination as studied by laser-flash photolysis of aqueous suspensions of TiO_2 particles in the absence of oxidizable compounds [36,37]. This discrepancy may either point to an incomplete kinetic scheme (e.g., H_2O_2 as an e^--scavenger formed from $HO_2^{\bullet}$ has been neglected [18]) or may indicate contributions from surface recombination processes induced by CH_3OH and species derived therefrom. The average steady-state number of e^-/h^+-pairs per TiO_2 particle was far less than unity in the present study. Therefore, a first-order rather than a second-order rate-law should hold for e^-/h^+-recombination [36]. However, a first-order rate law in conjunction with the above kinetic scheme cannot rationalize the observed dependence of Φ_{HCHO} on I_a. Finally, it should be noted that the above analysis cannot differentiate between mobile $OH^{\bullet}$, surface-bound $OH^{\bullet}$ (trapped holes) or photogenerated valence band holes [4,13–16] as the primary oxidizing species for CH_3OH, since in all cases a second-order rate law for recombination with photoelectrons is required in order to explain the finding shown in Fig. 5.

4.2. Comparison of the photocatalysts

The results presented above demonstrate different activity of the three photocatalysts for formation of formaldehyde from methanol. With respect to photonic efficiency, 2.4 nm TiO_2 particles are least active (Fig. 1 and Table 1). The quantum yield increases slightly on increasing the pH from 1 to 10 (Table 2). It is known that the potential of the conduction band edge of TiO_2 shifts in negative direction by −59 mV/pH [38]. Thus, the driving force for the rate-controlling reduction of oxygen (reaction (8) in the above kinetic scheme) increases with increasing pH. The rate of formaldehyde formation and the respective quantum yield should therefore be larger in alkaline solution. This is in agreement with observation. A recent study of 2.4 nm TiO_2 particles by laser-induced optoacoustic calorimetry in acidic solution indicated the formation of quasi-free $OH^{\bullet}$ [15]. These radicals are thought to abstract a H-atom from methanol in the present system, see reaction (9).

The photonic efficiency in the presence of P25 and Hombikat UV 100 depends strongly on pH and shows maxima near pH 8 and 10, respectively (Fig. 4). The pH controls the protonation state of the surface hydroxyl groups on TiO_2 which is governed by the following acid–base equilibria [19,39]

$$\equiv TiOH_2^+ \rightleftharpoons TiOH + H^+ \quad (pK_1) \quad (17)$$

$$\equiv TiOH \rightleftharpoons TiO^- + H^+ \quad (pK_2) \quad (18)$$

where the pH of zero point of charge is given by

$$pH_{zpc} = \tfrac{1}{2}(pK_1 + pK_2) \quad (19)$$

According to the above equilibria Kormann et al. [28] proposed a detailed model for the surface speciation of TiO_2 as a function of pH. The surface concentration of ≡TiOH passes a maximum with increasing pH as does the photonic efficiency for oxidation of methanol on P25 and Hombikat UV 100 (Fig. 4). This suggests that methanol is best adsorbed in the intermediate pH range where electroneutral ≡TiOH surface sites prevail which can form hydrogen-bonds with methanol. The surface concentration of methanol should be controlled by the pH via protonation/deprotonation of ≡TiOH surface sites and concomitant electrostatic binding of ions from $HClO_4$ and NaOH used for adjusting the pH as well as from KNO_3 present as an additive. Thus, adsorbed methanol would be displaced by ClO_4^- and NO_3^- in acidic solution and by Na^+ and K^+ in alkaline solution since these ions accumulate on the oppositely charged surface. In addition to pH-dependent adsorption of methanol which gives rise to the observed maximum of the photonic efficiency (Fig. 4), there is a monotonous increase of the efficiency with increasing pH as discussed above for the influence of the rate-controlling reduction of oxygen by photogenerated

electrons (shift by −59 mV/pH of the potential of the conduction band edge). The superposition of both effects explains why the pH values for maximal photonic efficiency (Fig. 4) are somewhat larger than the pH_{zpc} of ca. 6 for P25 [28] and bulk TiO_2 (anatase) powder [40].

The comparatively low activity of 2.4 nm TiO_2 particles can be attributed to a particle size effect. The primary particle size is ca. 9 nm for Hombikat UV 100 [27] and ca. 32–37 nm for the anatase component (80%) of P25 [27,41]. The particle size effect in pure TiO_2 photocatalysts has been discussed by Zhang et al. [41]. The quantum yield is limited by the undesired recombination of photogenerated charge carriers in the volume and at the surface of the particle. A decrease in particle size leads to the reduction of volume recombination because the migration time of photogenerated charge carriers to the surface is proportional to the square of the particle size [42]. Also, the overall number of surface active sites increases with decreasing particle size. This results in a higher interfacial charge transfer rate. Therefrom, the quantum yield should increase with decreasing particle size. However, when the particle size becomes very small, surface recombination becomes the dominating process [37,43,44]. This gives rise to the comparatively low quantum yield obtained here with 2.4 nm TiO_2 particles.

From the above considerations, an optimal particle size should exist in pure TiO_2 photocatalysts for maximal activity. Zhang et al. [41] demonstrated that the optimal particle size was ca. 10 nm for the photoassisted decomposition of chloroform. In the present study the photonic efficiency for oxidation of methanol was smaller at Hombikat UV 100 (9 nm particle size [27]) than at P25 (32–37 nm [27,41]) for catalyst loadings below 2.5 g l^{-1} and vice versa above 2.5 g l^{-1} (Fig. 3). Obviously, the activity of these commercial photocatalysts is not simply controlled by particle size. Additional factors such as microstructure, impurities, agglomeration and specific surface properties have to be taken into account. The comparatively high photoactivity of P25 has been attributed to the presence of the rutile phase [4] or, more likely to trace impurities of Fe(III) [41]. In fact, Fe(III)-doped TiO_2 nanoparticles have recently been shown to exhibit strongly enhanced photocatalytic activity for oxidation of methanol (Φ_{HCHO} up to approximately 0.15) [45].

In conclusion, the differences in activity of 2.4 nm TiO_2 particles and the commercial materials, P25 and Hombikat UV 100, for the photocatalytic oxidation of methanol as found in the present work cannot be interpreted by a simple unified model. Intrinsic properties rather than size effects have to be taken into account to understand the different activities of the commercial photocatalysts.

Acknowledgements

Chuan-yi Wang thanks the Alexander-von-Humboldt-Stiftung for a research fellowship grant and Mr. Sagawe and Mr. Hufschmidt for their help throughout this work. Financial support from the Deutsche Forschungsgemeinschaft (grants BA 1137/3-1, BA 1137/4-1 and DO 159/7-1) is gratefully acknowledged. Joseph Rabani and Detlef W. Bahnemann greatfully acknowledge the financial support of the work presented above through the European Union (Key action Sustainable Management and Quality of Water, Contract number EVK1-CT-2000-00077).

References

[1] D.F. Ollis, H. Al-Ekabi, Photocatalytic Purification and Treatment of Water and Air, Elsevier, Amsterdam, 1993.
[2] D. Bahnemann, J. Cunningham, M.A. Fox, E. Pelizzetti, N. Serpone, in: G.R. Helz, R.G. Zepp, D.G. Grosby (Eds.), Aquatic and Surface Photochemistry, Lewis Publishers, Boca Raton, FL, 1994, p. 261.
[3] A. Mills, R.H. Davis, D. Worsley, Chem. Soc. Rev. 22 (1993) 417.
[4] M.R. Hoffmann, S.T. Martin, W. Choi, D.W. Bahnemann, Chem. Rev. 95 (1995) 69.
[5] A. Heller, Acc. Chem. Res. 28 (1995) 503.
[6] P.V. Kamat, Chem. Rev. 93 (1993) 267.
[7] M.A. Fox, M.T. Dulay, Chem. Rev. 93 (1993) 341.
[8] P. Pichat, Catal. Today 19 (1994) 313.
[9] L.N. Lewis, Chem. Rev. 93 (1993) 2693.
[10] N. Serpone, E. Pelizzetti, Photocatalysis: Fundamentals and Applications, Wiley, New York, 1989.
[11] E. Pelizzetti, M. Schiavello, Photochemical Conversion and Storage of Solar Energy, Kluwer Academic Publishers, The Netherlands, 1991.
[12] D.W. Bahnemann, in: O. Hutzinger (Ed.), The Handbook of Environmental Chemistry, Vol. 2: Reactions and Processes, in: P. Boule (Ed.), Part L: Environmental Photochemistry, Springer, Berlin, 1999, p. 265.
[13] N. Serpone, R. Terzian, C. Minero, E. Pelizzetti, Adv. Chem. Ser. 238 (1993) 281.
[14] D.W. Bahnemann, M. Hilgendorff, R. Memming, J. Phys. Chem. B 101 (1997) 4265.
[15] K. Stopper, J.K. Dohrmann, Z. Phys. Chem. 214 (2000) 555.
[16] K. Ishibashi, A. Fujishima, T. Watanabe, K. Hashimoto, J. Photochem. Photobiol. A 134 (2000) 139.
[17] D. Bahnemann, A. Henglein, L. Spanhel, Faraday Discuss. Chem. Soc. 78 (1984) 151.
[18] L. Sun, J.R. Bolton, J. Phys. Chem. 100 (1996) 4127.
[19] C. Kormann, D.W. Bahnemann, M.R. Hoffmann, J. Phys. Chem. 92 (1988) 5196.
[20] H.G. Heller, J.R. Langan, J. Chem. Soc., Perkin Trans. I (1981) 341.
[21] E. Koivusalmi, E. Haatainen, A. Root, Anal. Chem. 71 (1999) 86.
[22] J.B. Goodenough, A. Hamnett, in: O. Madelung (Ed.), Landolt-Börnstein, New Series, Group III, Vol. 17g, Springer, Berlin, 1984, p. 147.
[23] R.J. Brandi, O.M. Alfano, A.E. Cassano, Environ. Sci. Technol. 34 (2000) 2623.
[24] R.J. Brandi, O.M. Alfano, A.E. Cassano, Environ. Sci. Technol. 34 (2000) 2631.
[25] M.I. Cabrera, O.M. Alfano, A.E. Cassano, J. Phys. Chem. 100 (1996) 20043.
[26] D. Bockelmann, M. Lindner, D.W. Bahnemann, in: E. Pelizzetti (Ed.), Fine Particles Science and Technology, Kluwer Academic Publishers, The Netherlands, 1996, p. 675.
[27] T. Hirakawa, Y. Nakaoka, J. Nishino, Y. Nosaka, J. Phys. Chem. B 103 (1999) 4399.
[28] C. Kormann, D.W. Bahnemann, M.R. Hoffmann, Environ. Sci. Technol. 25 (1991) 494.
[29] R. Memming, Top. Curr. Chem. 169 (1994) 106.
[30] P.A. Christensen, J. Eameaim, A. Hamnett, Phys. Chem. Chem. Phys. 1 (1999) 5315.

[31] G.E. Adams, J.W. Boag, B.D. Michael, Trans. Faraday Soc. 61 (1965) 1417.
[32] G.E. Adams, R.L. Willson, Trans. Faraday Soc. 65 (1969) 2981.
[33] H. Gerischer, Electrochim. Acta 38 (1993) 3.
[34] Ch.-M. Wang, A. Heller, H. Gerischer, J. Am. Chem. Soc. 114 (1992) 5230.
[35] H. Gerischer, A. Heller, J. Phys. Chem. 95 (1991) 5261.
[36] G. Rothenberger, J. Moser, M. Grätzel, N. Serpone, D.K. Sharma, J. Am. Chem. Soc. 107 (1985) 8054.
[37] N. Serpone, D. Lawless, R. Khairutdinov, E. Pelizzetti, J. Phys. Chem. 99 (1995) 16655.
[38] D. Duonghong, J. Ramsden, M. Grätzel, J. Am. Chem. Soc. 104 (1982) 2977.
[39] W. Stumm, J.J. Morgan, Aquatic Chemistry, Wiley/Interscience, New York, 1981, p. 625.
[40] G.A. Parks, Chem. Rev. 65 (1965) 177.
[41] Z. Zhang, C.-C. Wang, R. Zakaria, J.Y. Ying, J. Phys. Chem. B 102 (1998) 10871.
[42] A. Hagfeldt, M. Grätzel, Chem. Rev. 95 (1995) 49.
[43] M.A. Hines, P. Guyot-Sionnest, J. Phys. Chem. 100 (1996) 468.
[44] A.R. Kortan, R. Hull, R.L. Opila, M.G. Bawendi, M.L. Steigerwald, P.J. Carroll, L.E. Brus, J. Am. Chem. Soc. 112 (1990) 1327.
[45] C. Wang, D.W. Bahnemann, J.K. Dohrmann, Chem. Commun. (2000) 1539.